Langmuir
Article
pubs.acs.org/Langmuir

Adsorption of n-Pentane on Mesoporous Silica and Adsorbent Deformation

Gennady Yu. Gor,[*,†] Oskar Paris,[‡] Johannes Prass,[§] Patrícia A. Russo,[∥] M. Manuela L. Ribeiro Carrott,[∥] and Alexander V. Neimark[⊥]

[†]Department of Civil and Environmental Engineering, Princeton University, Princeton, New Jersey 08544, United States

[‡]Institute of Physics, Montanuniversitaet Leoben, Franz-Josef-Strasse 18, 8700 Leoben, Austria

[§]TimberTower GmbH, Vahrenwalder Strasse 7, 30165 Hannover, Germany

[∥]Centro de Química de Évora and Departamento de Química, Universidade de Évora, Colégio Luís António Verney, 7000-671 Évora, Portugal

[⊥]Department of Chemical and Biochemical Engineering, Rutgers University, 98 Brett Road, Piscataway, New Jersey 08854, United States

ABSTRACT: Development of quantitative theory of adsorption-induced deformation is important, e.g., for enhanced coalbed methane recovery by CO_2 injection. It is also promising for the interpretation of experimental measurements of elastic properties of porous solids. We study deformation of mesoporous silica by n-pentane adsorption. The shape of experimental strain isotherms for this system differs from the shape predicted by thermodynamic theory of adsorption-induced deformation. We show that this difference can be attributed to the difference of disjoining pressure isotherm, responsible for the solid–fluid interactions. We suggest the disjoining pressure isotherm suitable for n-pentane adsorption on silica and derive the parameters for this isotherm from experimental data of n-pentane adsorption on nonporous silica. We use this isotherm in the formalism of macroscopic theory of adsorption-induced deformation of mesoporous materials, thus extending this theory for the case of weak solid–fluid interactions. We employ the extended theory to calculate solvation pressure and strain isotherms for SBA-15 and MCM-41 silica and compare it with experimental data obtained from small-angle X-ray scattering. Theoretical predictions for MCM-41 are in good agreement with the experiment, but for SBA-15 they are only qualitative. This deviation suggests that the elastic modulus of SBA-15 may change during pore filling.

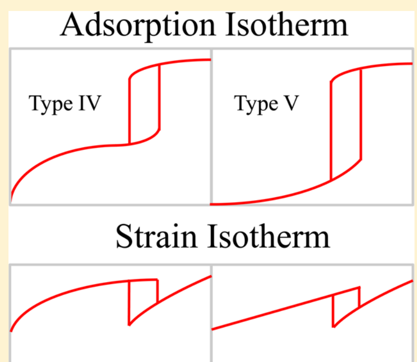

1. INTRODUCTION

Adsorption-induced deformation is expansion/contraction of porous solids caused by solid–fluid intermolecular forces during fluid adsorption. This phenomenon has been studied extensively during the 20th century, particularly in the seminal works of Meehan[1] and Bangham,[2] McIntosh,[3,4] Yates,[5] and Scherer[6] (brief review of these results is given in our earlier paper[7]). Understanding the mechanisms of adsorption-induced deformation is crucial for, e.g., enhanced coalbed methane recovery by CO_2 injection;[8−13] it also offers methods for measuring elastic properties of porous materials.[14,15] Therefore, recently the interest in this phenomenon has been reignited by both experimentalists[16−23] and theoreticians.[24−28]

Appearance of mesoporous molecular sieves (MMS) in 1990s has stimulated revolution in adsorption science.[29,30] Well-defined pore morphology, ordered arrangement of pores on 2D or 3D lattices, and narrow pore-size distribution of MMS made them a perfect system for verification of adsorption theories, particularly for the development of density functional theory.[31] We believe that MMS can also help developing quantitative theories of adsorption-induced deformation.

Most of the experimental data on adsorption-induced deformation are obtained by dilatometry, when the change of the volume or length of a macroscopic sample is measured.[18,21,23,32] However, deformation of a macroscopic sample is complicated: it may involve deformation of the pore space and deformation of the porous skeleton.[13,27] As a first step to understanding deformation of a macroscopic sample, it is necessary to verify theoretical predictions for deformation of the pore space of a single pore. Using in situ small-angle X-ray scattering (SAXS) one can measure how MMS lattice parameter changes during adsorption, and, therefore, obtain a strain isotherm, deformation of the pore lattice as a function of adsorbate pressure. Such data can be directly compared with the predictions of thermodynamic theory of adsorption-induced deformation,[7,33−35] based on the calculation of solvation pressure, i.e., the pressure which the adsorbed fluid exerts on a pore wall.

Received: April 23, 2013
Revised: June 9, 2013
Published: June 12, 2013

Table 1. Sample Properties[a]

sample	A_{BET} ($m^2\ g^{-1}$)	A_s ($m^2 g^{-1}$)	A_{ext} ($m^2\ g^{-1}$)	V_p ($cm^3\ g^{-1}$)	V_{mp} ($cm^3\ g^{-1}$)	D_p (nm)
TK800	148	149	149	0	0	n/a
SBA-15-I	937	621	18	0.94	0.13	7.87
SBA-15-II	730			1.01		8.14
MCM-41	905			0.659		3.54

[a] A_{BET}, specific surface area determined by the BET method; A_s, A_{ext}, V_p, V_{mp}, specific surface area, external surface area, pore volume, and micropore volume, respectively, determined by the α_s method; D_p, pore size determined by NLDFT. (Some of the parameters for SBA-15-II and MCM-41 were not determined.)

In our previous works[7,35] we derived theoretical predictions for solvation pressure for nitrogen and argon, gases typically used for porosimetry. However, in situ SAXS measurements in refs 16 and 17 were conducted at room temperature. The groups of Findenegg and Paris used water,[17] perfluoropentane, and n-pentane[16,19] for such experiments. When n-pentane is used as adsorptive, the behavior of the resulting strain isotherm at low pressures (prior to capillary condensation) almost linearly increases with pressure,[16,19] which is qualitatively different from the concave shape predicted by Gor and Neimark for nitrogen or argon adsorption on silica.[7,35] The main question to be addressed in this paper is whether the thermodynamic theory of adsorption-induced deformation of mesoporous solids[7,35] is capable of predicting deformation behavior of silica caused by n-pentane adsorption at low pressures.

We present an extension of our macroscopic theory of adsorption-induced deformation of mesoporous solids[7,35] for weak solid−fluid interactions, which is the case for n-pentane adsorption on silica. The predictions for a strain isotherm are based on the calculation of solvation pressure. Solvation pressure is derived following the method by Gor and Neimark[7,35] based on Derjaguin−Broekhoff−de Boer (DBdB) theory of capillary condensation.[36−38] This method represents the adsorbate chemical potential by two terms related to the capillary and disjoining pressures. While the former is simply calculated using the value of liquid−vapor surface tension, the latter (representing the solid−fluid interactions) is based on experimental data of adsorption on nonporous surface. We measured a reference adsorption isotherm for n-pentane on nonporous TK800 silica at 298 K. We show that a two-parametric Frenkel−Halsey−Hill (FHH) equation[39−41] is not capable to fit this isotherm. Therefore, we used a four-parametric exponential disjoining pressure isotherm[42] for fitting our data. We show that, unlike the FHH isotherm, the four parametric expression is capable of approximating the reference isotherm within the whole range of pressures. The extension of the macroscopic theory of adsorption-induced deformation allows us to explain both previously published[16,19] and new SAXS data on deformation of MCM-41 and SBA-15 silica caused by n-pentane adsorption. Particularly, the theory is now capable of predicting the near-linear strain behavior at low pressures, observed in the experiment. We also find peculiar differences between deformation of samples with high (SBA-15) and low (MCM-41) microporosity. Finally, our study supports the recent findings of Prass et al.[19] showing that "apparent lattice deformation" (sharp peaks around capillary condensation/evaporation pressures) is an artifact of the SAXS technique and it is not related to a real deformation of the pore.

The paper is organized as follows: In section 2 we briefly describe the adsorption experiments and in situ small-angle X-ray scattering technique, and how it can be applied for measuring the adsorption-induced deformation. Then we give a short overview of macroscopic theory of adsorption-induced deformation of mesoporous solids and extend it to the case of weak solid−fluid interactions. In section 3 the results are given; we start from analysis of the disjoining pressure isotherm of n-pentane on reference silica surface. Then we use this isotherm to calculate solvation pressure and elastic strain for porous samples and compare it with previously published and newly reported experimental data. The results are discussed in section 4. Section 5 presents the conclusion.

2. METHODS

2.1. Experiment. The n-pentane adsorption−desorption isotherms, at 298 K, on TK800 silica and a SBA-15-I silica, were determined gravimetrically in an apparatus equipped with a CI Electronics MK2 vacuum microbalance coupled to a Disbal control unit. Pressure was measured with Edwards Barocel 600 capacitance manometer. The temperature was controlled within ±0.1 K using a Grant LTD thermostat and a Masterflex peristaltic pump. Prior to the adsorption experiments, the n-pentane (99%, Lab-Scan) was purified by double distillation and then outgassed in vacuum by repeated freeze−thaw cycles, and the samples were outgassed at 473 K for 8 h with a heating rate of 5 K min^{-1}. The results of characterization by X-ray diffraction and nitrogen adsorption−desorption at 77 K (experimental details as previously described[43]) were presented in a previous paper for the present SBA-15-I sample[44] which has a pore size of 7.87 nm (by NLDFT method), but the n-pentane adsorption−desorption isotherms have not been reported yet. Table 1 summarizes main properties of the samples.

The nonporous TK800 considered in this work is pure silica (National Physical Laboratory, United Kingdom), and it is arc silica, a type of pyrogenic silica, on which nitrogen adsorption isotherm of Type II, reversible up to ∼$0.85P_0$, was obtained. The nitrogen adsorption isotherm was analyzed using the FHH equation, being obtained a value of 2.72, in remarkable agreement with that previously reported for the adsorption of nitrogen at 77 K on Degussa TK800[45] and also on a variety of nonporous solids.[46,47] Furthermore, the corresponding α_S plot, using as reference the published standard data on nonporous hydroxylated silica,[46,47] presented a long linear section which could be back-extrapolated to the origin, and the specific surface area is in close agreement with the value obtained by the BET method as seen in Table 1. On the basis of these results we can consider that the TK800 used in the present study is nonporous.

Strain isotherms of two MMS samples were measured at room temperature (290 K) using synchrotron radiation X-rays at the Helmholtz Center Berlin at the BESSY II facility. Details of the in situ sorption setup, the measurement strategy, and the data evaluation are given in previous papers.[16,17] MCM-41 sample with 3.54 nm pore diameter,[48] and SBA-15-II sample with 8.14 nm diameter[49] (both determined by the NLDFT method from N_2 adsorption isotherms), were used for the experiments. The MCM-41 and the SBA-15-II samples have similar mesoporosity of 62% and 56%, respectively,[17] but the SBA-15-II additionally contains about 13% porosity corresponding to micropores within the mesopore walls.[49]

2.2. Theory. Gas adsorption in a mesoporous sample can be fairly well described by Derjaguin–Broekhoff–de Boer (DBdB) theory of capillary condensation.[36−38] DBdB theory was verified for argon and nitrogen adsorption on silica against more precise theories, based on molecular density functional theory, and it gives quantitative predictions for pores larger than 7–10 nm.[50] In our recent work[35] we showed that predictions of DBdB theory for solvation pressure isotherms are in good agreement with predictions based on microscopic methods (QSDFT) for argon and nitrogen in 8.2 nm silica pore. For smaller pores (4 nm), although the deviation of predictions for points of capillary condensation and evaporation is noticeable, the solvation pressure curve calculated on the basis of DBdB theory is still close to the one based on QSDFT.[35]

Within DBdB theory the adsorbate is considered as a macroscopic liquid film. The chemical potential of this film differs from the chemical potential of the bulk liquid and is given by[36]

$$\mu = -\left(\Pi(h) + \frac{\gamma}{R - h}\right)V_L \tag{1}$$

The molar volume of the adsorbed fluid V_L is assumed to be the same as that of the bulk liquid. The two terms in the brackets are related to the solid–fluid interactions and film curvature respectively. The latter term is just the Laplace pressure at the curved liquid–vapor interface: γ is the liquid–vapor surface tension, R is the radius of the pore, h is the thickness of the liquid film. The key term, however, is the first term, Derjaguin's disjoining pressure Π. Disjoining pressure isotherm $\Pi = \Pi(h)$ can be obtained from the experimental data on adsorption on reference nonporous solid, and usually it is approximated with two-parametric Frenkel–Halsey–Hill (FHH) equation[39−41]

$$\Pi(h) = \frac{R_g T}{V_L}\frac{k}{(h/h_0)^m} \tag{2}$$

Here, R_g is the gas constant, T is the absolute temperature, $h_0 = 1$ Å, and k and m are the dimensionless parameters. FHH eq 2 approximates fairly well disjoining pressure of nitrogen and argon adsorption on silica.[50] Another type of disjoining pressure isotherm, widely used for describing adsorption on silica and glass surfaces, is the so-called "isotherm of structural forces",[51,52] given by two-parametric exponential expression:

$$\Pi(h) = \Pi_1 \exp\left(-\frac{h}{\lambda_1}\right) \tag{3}$$

Here Π_1 and λ_1 are the parameters derived from experiments, which have the dimension of pressure and length, respectively. Equation 3 is found more suitable for hydrocarbons than the FHH equation; as such, Schlangen et al.[53] and Ravikovitch et al.[54] used eq 3 to study n-alkanes, cyclohexane, and toluene adsorption on silica. Often, to better fit the experimental data, a more complex four-parametric expression is used[42,55,56]

$$\Pi(h) = \Pi_1 \exp\left(-\frac{h}{\lambda_1}\right) + \Pi_2 \exp\left(-\frac{h}{\lambda_2}\right) \tag{4}$$

where parameters Π_1, λ_1, Π_2, and λ_2 are determined from experimental data.

DBdB theory is able to predict the capillary condensation/evaporation hysteresis, which is typical for large mesopores. The critical film thickness h_c at the capillary condensation point is determined from the condition of maximum of chemical potential as a function of h (eq 1)

$$\left.\frac{d\Pi(h)}{dh}\right|_{h=h_c} + \frac{\gamma}{(R - h_c)^2} = 0. \tag{5}$$

The capillary evaporation takes place close to equilibrium, and therefore, the disjoining pressure can be predicted from the Maxwell equal area rule (when the grand potentials of the filled pore with meniscus equal the grand potential of the pore with the adsorbed liquid film of the thickness h_e). This condition gives Derjaguin equation[38]

$$\Pi(h_e) - \frac{\gamma}{R - h_e} = \frac{1}{(R - h_e)^2}\int_{h_e}^{R}(R - h')\Pi(h')\,dh' \tag{6}$$

Thus, given the pore radius R, adsorbate properties (surface tension γ and molar volume V_L), and adsorbate–adsorbent interactions, DBdB theory predicts the full adsorption isotherm. Before capillary condensation, the adsorbed film thickness h (and the filling fraction) is related to the gas pressure P through eq 1 and

$$\mu = R_g T \ln(P/P_0) \tag{7}$$

where P_0 is the pressure of saturated vapor at temperature T. After the capillary condensation, the pore is assumed to be fully filled with the bulk liquid.

DBdB theory has been used for calculation of adsorption isotherms for decades, but just recently we have found that it can be employed for predicting the adsorption-induced deformation.[7] Elastic strain ε of a pore is related to the solvation pressure f_s in the pore through Hooke's law

$$\varepsilon = \varepsilon_0 + f_s/M \tag{8}$$

where ε_0 is the prestrain (at the dry state) and M is an elastic modulus of the pore system. This is a similar pragmatic definition, as in,[17] where the ratio between the Laplace pressure in the pores and the measured pore lattice strain in MCM-41 and SBA-15 materials was denoted "pore-load modulus". It should be noted that the pore load modulus is in general different from the bulk modulus of the system, as it corresponds to a completely different loading situation and possibly also a different measure of deformation. For instance in the case of MCM-41 and SBA-15, the pore load modulus corresponds to the ratio between an internal pressure in each single pore in a hexagonal pore lattice and the measured pore lattice strain. If the geometry of the system is known, this pore load modulus can be related to common elastic parameters of the pore walls, by, e.g., finite element continuum mechanical calculations.[17] The problem of deriving the macroscopic deformation of porous materials in response to capillary forces has often been treated very superficially, and has been critically discussed recently by Weissmuller et al.[57]

The solvation pressure is the pressure which the film of adsorbed fluid exerts on a pore wall. It is often referred to as "disjoining pressure". However, we would like to avoid this term, to clearly distinguish it from the original Derjaguin's notion of disjoining pressure, determined for a flat surface. Solvation pressure equals $f_s = \sigma - P$, where the adsorption stress σ for cylindrical pore geometry is calculated from the simple thermodynamic relation[7,33]

$$\sigma = -\left(\frac{\partial\Omega}{\partial V}\right)_{\mu,T} = -\frac{1}{2\pi RL}\left(\frac{\partial\Omega}{\partial R}\right)_{\mu,T} \tag{9}$$

Here Ω is the grand potential of the pore with adsorbate in it; L is the length of the cylindrical pore. In our previous work we employed DBdB theory to derive analytical expressions for the grand potential Ω and adsorption stress σ,[7] which gives for the pore filled with fluid

$$\sigma = -\frac{\gamma_{sl}}{R} + \frac{R_g T}{V_L}\ln\left(\frac{P}{P_0}\right) + P_0 \tag{10}$$

where γ_{sl} is the surface tension at the solid–liquid interface. The simplicity of eq 10 allows one to easily determine the elastic modulus M from the experimental adsorption strain for the filled pore with condensed fluid. The logarithmic dependence of solvation pressure on the gas pressure for the filled pores has been known for decades[58] and has been used for determination of the elastic modulus previously.[15,32]

For the pore with adsorbed film on the wall the adsorption stress is given by (see ref 7 and Supporting Information therein for details)

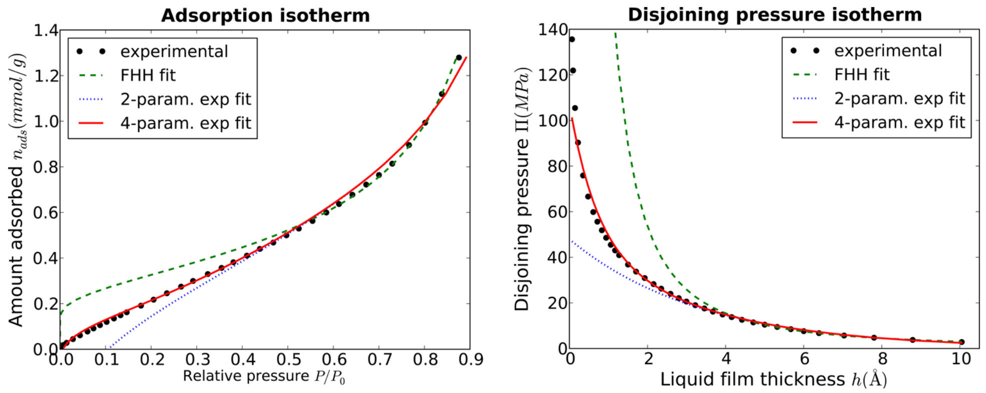

Figure 1. Adsorption of n-pentane on nonporous silica surface (TK800 silica) at 298 K. (Left) Reference adsorption isotherm: experimental data and fitting using various expressions for disjoining pressure. (Right) Disjoining pressure isotherm derived from experimental data and results of fitting of the theoretical disjoining pressure isotherms. Only the four-parametric disjoining pressure isotherm with two exponential terms (eq 4) allows achieving a good fit within the whole range of pressures.

$$\sigma = -\frac{\gamma_{sl}}{R} - \frac{\gamma}{R-h} - \frac{h}{R}\Pi(h) - \frac{1}{R}\int_h^\infty \Pi(h')\,dh' \tag{11}$$

Since eq 11 stems from eq 1, it includes contributions related to both solid−fluid interactions and curvature of the adsorbed film. The solid−fluid part, written in terms of disjoining pressure, can be interpreted in terms of the Bangham effect.[7] In order to calculate the solvation pressure prior to capillary condensation, eq 11 has to be complemented with disjoining pressure isotherm $\Pi(h)$. Adsorption stress for FHH disjoining pressure isotherm was obtained previously.[7] If the disjoining pressure has the form of eq 4, the adsorption stress in the region prior to capillary condensation is given by

$$\sigma = -\frac{\gamma_{sl}}{R} - \frac{\gamma}{R-h} - \left\{\Pi_1\left(\frac{h+\lambda_1}{R}\right)\exp\left(-\frac{h}{\lambda_1}\right) + \Pi_2\left(\frac{h+\lambda_2}{R}\right)\exp\left(-\frac{h}{\lambda_2}\right)\right\} \tag{12}$$

To calculate σ for two-parametric exponential disjoining pressure isotherm (eq 3), only the first term in the brackets in eq 12 is used, since the second term equals zero. Equations 8, 10, and 12 are used below to calculate the strain isotherms.

3. RESULTS

Adsorption stress σ, solvation pressure f_s, and, therefore, the elastic strain ε strongly depend on the interactions between the solid and fluid molecules, which are determined by the disjoining pressure $\Pi(h)$. Analytical approximation for the disjoining pressure isotherm $\Pi(h)$ can be obtained from the reference adsorption isotherm on nonporous surface. We measured n-pentane adsorption isotherm on nonporous TK800 silica at 298 K, and these data are displayed as filled circles in the left panel of Figure 1. We derive the thickness h of the adsorbed film from the values of n_{ads} (amount adsorbed per unit mass of a sample) using the following simple relation

$$h = \frac{n_{ads}}{S_A}V_L \tag{13}$$

where specific surface area S_A of the present TK800 silica as determined by nitrogen adsorption at 77 K is 148 m^2/g and the molar volume V_L of adsorbed n-pentane was calculated as $V_L = \mu/\rho$ (μ = 72.2 g/mol is the molar mass of pentane and ρ = 621 kg/m^3 is its bulk liquid density at 298 K). The experimental values of disjoining pressure $\Pi(h)$ are obtained from the relative pressure P/P_0 using

$$\Pi(h) = -\frac{R_g T}{V_L}\ln\left(\frac{P}{P_0}\right) \tag{14}$$

The experimental dependence of disjoining pressure on the thickness of adsorbed film is shown in the right panel of Figure 1 as filled circles.

We use three different analytical expressions to fit the experimental disjoining pressure curve: two-parametric FHH isotherm (eq 2), two-parametric exponential isotherm (eq 3), and four-parametric expression, consisting of two exponential terms (eq 4). Right panel of Figure 1 shows that both two-parametric formulas give a good fit for film thickness h in the range from 3−4 to 11 Å. Attempts to fit below 3 Å caused substantial deterioration of prediction at large thickness. However, the four-parametric expression for disjoining pressure provides good fit in the whole range of film thickness, even below 1 Å. The results of fitting of experimental adsorption isotherm and disjoining pressure isotherm by four-parametric expression eq 4 are represented with solid lines in left and right panels of Figure 1, respectively.

On the basis of our fitting we obtain the following values of the parameters to be used for modeling n-pentane adsorption on silica surface: FHH isotherm parameters k = 8.70, m = 1.79; exponential isotherm (eq 4) parameters Π_1 = 47.9 MPa, λ_1 = 3.38 Å, Π_2 = 59.5 MPa, λ_2 = 0.69 Å. When using two-parametric exponential expression (eq 3) we obtain the same parameters as Π_1 and λ_1 given above.

After we fit the parameters for disjoining pressure isotherm, we can employ the DBdB theory to calculate n-pentane adsorption isotherm on a mesoporous sample. Figure 2 gives the experimental isotherm for n-pentane adsorption at 298 K on SBA-15-I with pore size 7.87 nm (●) and the theoretical DBdB isotherm for cylindrical pore of this size (—). The liquid−vapor surface tension of pentane γ is taken 15.28 mN/m from ref 59. The theoretical isotherm is shifted upward by 0.18 to take into account the filling of micropores; this correction is close to the relative volume of micropores calculated for SBA-15-I sample by α_s method.[44] The effective diameter of n-pentane molecule is ∼4 Å, approximating it by a sphere.[26] According to the disjoining pressure isotherm, 4 Å thickness (filling of the monolayer) corresponds to the relative pressure P/P_0 = 0.5. (This is in line with the good fit of FHH isotherm at the pressures P/P_0 > 0.5.) The deviations in Figure 2 correspond to relative pressures below 0.3, i.e., before the

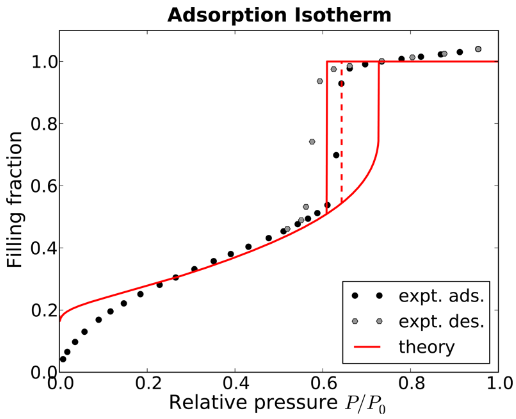

Figure 2. Adsorption of n-pentane on SBA-15-I silica (pore size 7.87 nm) at 298 K. Theoretical isotherm (—) is obtained using DBdB theory with the disjoining pressure isotherm eq 4. Prediction of DBdB theory for capillary condensation pressure noticeably deviates from the experimental value (---). However, the pressure of equilibrium transition and the isotherm in the region of multilayer adsorption are predicted accurately.

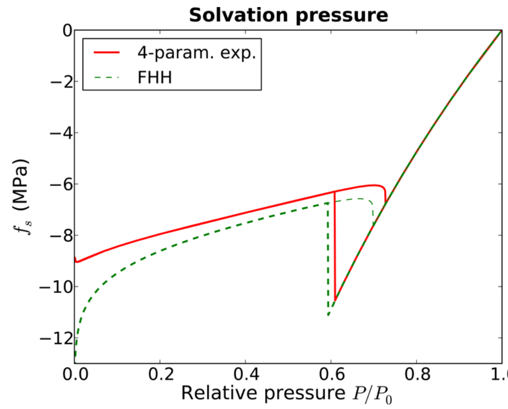

Figure 3. Theoretical predictions of solvation pressure in the cylindrical silica pore 7.87 nm as a function of relative pressure of n-pentane (at 298 K). Dashed line shows calculations based on FHH disjoining pressure isotherm eq 2; solid line shows calculations based on four-parametric exponential expression for disjoining pressure isotherm eq 4. At low adsorbate pressure there is a noticeable difference between two predictions: while the FHH isotherm leads to a concave solvation pressure curve, the exponential disjoining pressure gives almost linear behavior.

monolayer completion. Therefore, these deviations can be addressed to gradual filling of the micropores. The agreement between the slope of theoretical isotherm and experimental in the region of multilayer adsorption suggests that TK800 is a suitable reference surface. The prediction for the position of equilibrium capillary evaporation, determined by eq 6, is close to the experimental points. The capillary condensation pressure (determined by eq 5) is noticeably overpredicted. The capillary condensation corresponding to the experimental value is shown by the dashed line. Such deviation could cause a problem if theoretical isotherms would be used in a kernel for calculating pore-size distributions. However, as we will see below, it is not critical for predicting adsorption-induced deformation.

We use our theory to calculate the solvation pressure isotherm for the sample discussed above. In our calculations we use both FHH disjoining pressure isotherm (eq 2) and the four-parametric exponential expression (eq 4). The results are shown by dashed and solid lines, respectively, in Figure 3. The solvation pressure for the pore filled with capillary condensate is calculated using eq 10, which does not depend on disjoining pressure isotherm. Therefore, we get the same predictions for these parts. Predictions for capillary condensation and evaporations pressures are close and the solvation pressure at relative adsorbate pressure above 0.2. However, the calculations noticeably differ in the low pressure region.

We calculate the solvation pressure for two systems: a silica pore of 3.4 nm size and a silica pore of 8.14 nm. These diameters correspond to the MCM-41 and SBA-15-II samples used in experiments by the Paris group[16,19] within the acceptable accuracy of the adsorption methodology. We use the part of the solvation pressure curve for the filled pore (after capillary condensation), determined by eq 10, to fit the prestrain ε_0 and the elastic modulus M using eq 8. For the MCM-41 sample we get M = 14.6 GPa; for the SBA-15-II sample we get M = 6.4 GPa. This is in good agreement with the values reported in ref 17 calculated from the data on other adsorbates. We do not use the solid−liquid surface tension γ_{sl} in the calculation of solvation pressure; instead, it is taken into account by the constant vertical shift of the resulting strain isotherm. Figure 4 presents the results of our calculations along with the strain of the pore, experimentally measured by SAXS. The adsorption data for MCM-41 is from ref 16, desorption data for SBA-15-II is from ref 19, and desorption data for MCM-41 and adsorption data for SBA-15-II have not been reported elsewhere. As we mentioned above, the DBdB theory does not predict the points of capillary condensation/evaporation precisely. However, Figure 4 shows that the macroscopic theory of adsorption-induced deformation based on DBdB theory predicts the strain isotherms close to the experimental data.

4. DISCUSSION

Experimental strain isotherms for n-pentane adsorption on silica at low pressures behave differently than our recent theory[35] predicts. However, in ref 35 the predictions were calculated for argon and nitrogen adsorption on silica, not for n-pentane. Here we show that the difference in strain behavior is due to the difference in solid−fluid interactions. Within the macroscopic theory of adsorption-induced deformation, the solid−fluid interactions are taken into account through the disjoining pressure isotherm. We show that the FHH isotherm is incapable of describing n-pentane adsorption. We use four-parametric exponential disjoining pressure isotherm, which better represents weak solid−fluid interactions. First we show that, unlike FHH, such an isotherm excellently approximates the experimental adsorption data on a nonporous surface within the whole range of pressures. From this approximation we derive parameters, which we employ further in our calculations. We show that using these parameters we can reproduce the experimental adsorption isotherm in the region of multilayer adsorption (before capillary condensation). The prediction for the pressure of capillary condensation deviates from the experimental value. However, this deviation does not affect the predictions for solvation pressure.

We calculate the solvation pressure for a pore of 7.87 nm using the theory presented in ref 7. We compare predictions based on FHH disjoining pressure isotherm and four-parametric exponential disjoining pressure isotherm. We show that at the relative adsorbate pressure higher than 0.2 the predictions based on both disjoining pressure isotherm almost

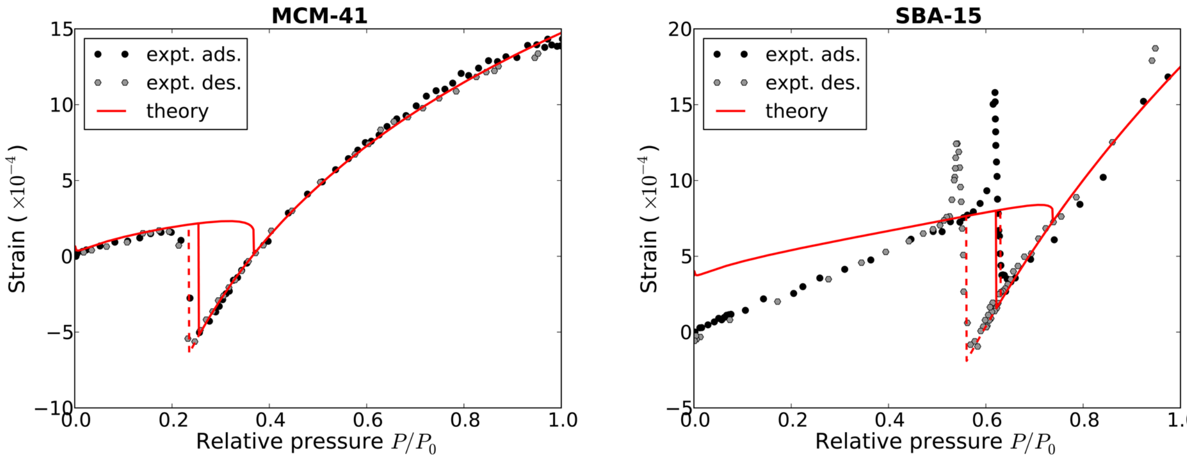

Figure 4. n-Pentane adsorption-induced deformation of mesoporous silica. (Left) MCM-41, experimental data (adsorption branch, black markers; desorption, gray markers), theoretical predictions with capillary condensation and evaporation points predicted from DBdB theory (—), predictions based on experimental value of capillary condensation pressure (---). (Right) SBA-15-II experimental data (adsorption branch, black markers; desorption, gray markers), theoretical predictions (—), theoretical predictions based on experimental values of capillary condensation and evaporation pressures (---).

coincide. However, at the adsorbate pressure lower than 0.2 the calculations based on FHH lead to the concave shape of the solvation pressure curve. The predictions based on four-parametric exponential disjoining pressure isotherm give the near-linear behavior, which is observed in experiments.

Similarly to classification of adsorption isotherms,[46,47] we can classify the strain isotherms based on the strength of solid−fluid interactions. Figure 5 presents Type IV and Type V adsorption

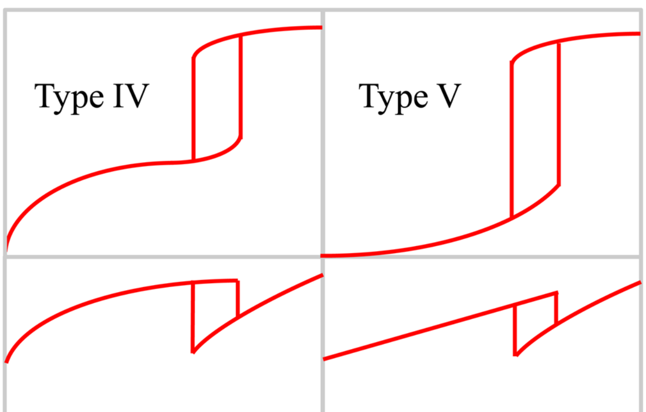

Figure 5. Classification of adsorption isotherms for mesoporous materials (top) and corresponding strain isotherms for adsorption-induced deformation (bottom). In the case of strong solid−fluid interactions at low pressures, substantially more fluid gets adsorbed (concave adsorption isotherm), and they also cause higher expansion of a sample (concave strain isotherm).

isotherms, which are characteristic isotherms for fluid adsorption in mesoporous solids for strong and weak solid−fluid interactions, respectively. It is possible that when the solid−fluid interactions are very weak, the expansion of a sample before capillary condensation is negligible, so the strain isotherm has a very moderate slope. Such strain isotherms have been reported recently by Dendooven et al.[60] for toluene adsorption on silica.

Results of our calculations can be compared directly with the strain isotherms derived from SAXS experiments. We consider experimental data for n-pentane adsorption on two MMS samples MCM-41 and SBA-15-II. We calculate solvation pressure for the pore sizes corresponding to these samples and get the elastic strain by employing Hooke's law. For MCM-41 the pressures at capillary condensation/evaporation do not agree well with experiment, which is expected for small mesopores. However, the strain isotherm fits very well.

The experimental strain isotherm for n-pentane adsorption on SBA-15-II, shown in Figure 4, has a well pronounced hysteresis loop. Adsorption isotherms for large channel-like mesopores (larger than ∼4 nm in diameter) are known to have hysteresis. The reasons for hysteresis for such systems are the following:[61] the capillary condensation takes place when the fluid film adsorbing on the walls reaches the limit of its thermodynamic stability, the capillary evaporation (desorption) takes place as the equilibrium transition, which corresponds to noticeably lower gas pressure then the capillary condensation. The hysteresis on the strain isotherm on SBA-15 is the direct consequence of adsorption hysteresis. Thus, the drop in the strain at lower pressure corresponds to equilibrium capillary evaporation, and the drop of the strain at the higher pressure corresponds to the capillary condensation.

For SBA-15 the capillary condensation/evaporation are closer, but the calculated strain isotherm reproduces the experimental curve only qualitatively. This mismatch may look surprising, given the good agreement for MCM-41. The deviation of theoretical predictions for strain from the experimental stress isotherm on SBA-15 sample suggests that its elastic properties change during pore filling. Unlike MCM-41 silica, the walls of SBA-15 include a substantial amount of micropores (so-called "corona"). Since the stiffening effect is pronounced in SBA-15 and is not seen in MCM-41, it may be due to filling of microporous corona of SBA-15. This effect is in line with the recent results of Coasne et al., who predicted the stiffening of microporous materials upon adsorption from molecular simulations.[62] The effects related to the change of elastic properties cannot be modeled within our current approach.

From the comparison of experimental and theoretical strain isotherms for SBA-15 silica we can make another important observation. The spikes observed in the experiment around capillary condensation and evaporation points are not seen on the theoretical curve. It confirms the conclusion of the previous study by Prass et al.[19] that the spikes are artifacts of the SAXS method.

When modeling deformation of microporous materials, for calculation of the pressure in the pores Grand Canonical Monte Carlo (GCMC) simulations are often used.[10,12,25,28,34,63] Schoen et al. used GCMC for calculating the strain isotherm for mesoporous MCM-41.[26] However, Monte Carlo simulations cannot be readily employed for calculation of the strain isotherm for SBA-15. The pore size of 7−8 nm is relatively large, so Monte Carlo simulations for such system are too computationally expensive. NLDFT or QSDFT methods[31] also cannot be used, since they are developed for simple Lennard-Jones molecules, which is not the case for n-pentane. Therefore, currently our macroscopic approach is presumably the best way to predict deformation of large mesopores induced by adsorption of complex fluids.

5. CONCLUSION

We have studied deformation of mesoporous silica induced by adsorption of n-pentane. The shape of experimental strain isotherms at low pressure qualitatively differs from the shape predicted by our thermodynamic theory of adsorption-induced deformation of mesoporous solids.[7,35] Therefore it was questioned whether this theory is capable of explaining the experiments with n-pentane. We have found that the shape of a strain isotherm at low pressures is governed by the strength of solid−fluid interaction, very similar to the shape of an adsorption isotherm at low pressures. We have extended our theory for the case of weak solid−fluid interactions and have shown that this extension predicts near-linear behavior of a strain isotherm at low pressure, which is also observed in experiments for n-pentane. We have compared the predictions of our theory with recently published and new strain isotherm for n-pentane adsorption on mesoporous silica, obtained using SAXS technique. We have found good agreement between the theory and experiment for strain isotherm for MCM-41 silica. However, for SBA-15 silica the agreement is only qualitative. We believe that the deviation of theoretical predictions for SBA-15 from the experimental strain is due to the change of elastic properties of the sample. Since this change has not been observed for MCM-41, it may be related to the microporous walls of SBA-15.

More conclusions on the mechanisms of adsorption-induced deformation could be made if more experimental data were available for MMS. Strain isotherms for argon and nitrogen adsorption are of particularly high interest, because they could be verified against the calculations based on the benchmark methods NLDFT or QSDFT.

■ AUTHOR INFORMATION

Corresponding Author

*E-mail: ggor@princeton.edu.

Notes

The authors declare no competing financial interest.

■ ACKNOWLEDGMENTS

A.V.N. acknowledges partial support from the Rutgers NSF ERC "Structured Organic Particulate Systems". M.M.L.R.C. acknowledges the Fundação para a Ciência e a Tecnologia (FCT, Portugal) for partial financial support (Strategic Project PEst-OE/QUI/UI0619/2011).

■ REFERENCES

(1) Meehan, F. T. The expansion of charcoal on sorption of carbon dioxide. *Proc. R. Soc. London, Ser. A* **1927**, *115*, 199−207.

(2) Bangham, D. H.; Fakhoury, N. The expansion of charcoal accompanying sorption of gases and vapours. *Nature* **1928**, *122*, 681−682.

(3) Amberg, C. H.; McIntosh, R. A study of adsorption hysteresis by means of length changes of a rod of porous glass. 1952, *30*, 1012−1032.

(4) Haines, R. S.; McIntosh, R. Length changes of activated carbon rods caused by adsorption of vapors. *J. Chem. Phys.* **1947**, *15* (1), 28−38.

(5) Yates, D. J. C. The expansion of porous glass on the adsorption of non-polar gases. *Proc. R. Soc. London, Ser. A* **1954**, *224* (1159), 526−544.

(6) Scherer, G. W. Dilatation of porous-glass. *J. Am. Ceram. Soc.* **1986**, *69* (6), 473−480.

(7) Gor, G. Y.; Neimark, A. V. Adsorption-induced deformation of mesoporous solids. *Langmuir* **2010**, *26* (16), 13021−13027.

(8) Pan, Z. J.; Connell, L. D. A theoretical model for gas adsorption-induced coal swelling. *Int. J. Coal Geol.* **2007**, *69* (4), 243−252.

(9) Battistutta, E.; van Hemert, P.; Lutynski, M.; Bruining, H.; Wolf, K. H. Swelling and sorption experiments on methane, nitrogen and carbon dioxide on dry Selar Cornish coal. *Int. J. Coal Geol.* **2010**, *84* (1), 39−48.

(10) Kowalczyk, P.; Furmaniak, S.; Gauden, P. A.; Terzyk, A. P. Methane-induced deformation of porous carbons: From normal to high-pressure operating conditions. *J. Phys. Chem. C* **2012**, *116* (2), 1740−1747.

(11) Vandamme, M.; Brochard, L.; Lecampion, B.; Coussy, O. Adsorption and strain: The CO_2-induced swelling of coal. *J. Mech. Phys. Solids* **2010**, *58* (10), 1489−1505.

(12) Brochard, L.; Vandamme, M.; Pellenq, R. J. M.; Fen-Chong, T. Adsorption-induced deformation of microporous materials: Coal swelling induced by CO_2-CH_4 competitive adsorption. *Langmuir* **2012**, *28* (5), 2659−2670.

(13) Brochard, L.; Vandamme, M.; Pellenq, R. J. M. Poromechanics of microporous media. *J. Mech. Phys. Solids* **2012**, *60* (4), 606−622.

(14) Dourdain, S.; Britton, D. T.; Reichert, H.; Gibaud, A. Determination of the elastic modulus of mesoporous silica thin films by X-ray reflectivity via the capillary condensation of water. *Appl. Phys. Lett.* **2008**, *93* (18), 183108.

(15) Mogilnikov, K. P.; Baklanov, M. R. Determination of Young's modulus of porous low-k films by ellipsometric porosimetry. *Electrochem. Solid State Lett.* **2002**, *5* (12), F29−F31.

(16) Guenther, G.; Prass, J.; Paris, O.; Schoen, M. Novel insights into nanopore deformation caused by capillary condensation. *Phys. Rev. Lett.* **2008**, *101* (8), 086104.

(17) Prass, J.; Muter, D.; Fratzl, P.; Paris, O. Capillarity-driven deformation of ordered nanoporous silica. *Appl. Phys. Lett.* **2009**, *95* (8), 083121.

(18) Balzer, C.; Wildhage, T.; Braxmeier, S.; Reichenauer, G.; Olivier, J. P. Deformation of porous carbons upon adsorption. *Langmuir* **2011**, *27* (6), 2553−2560.

(19) Prass, J.; Muter, D.; Erko, M.; Paris, O. Apparent lattice expansion in ordered nanoporous silica during capillary condensation of fluids. *J. Appl. Crystallogr.* **2012**, *45* (4), 798−806.

(20) Sorenson, S. G.; Payzant, E. A.; Gibbons, W. T.; Soydas, B.; Kita, H.; Noble, R. D.; Falconer, J. L. Influence of zeolite crystal expansion/contraction on NaA zeolite membrane separations. *J. Membr. Sci.* **2011**, *366* (1−2), 413−420.

(21) Shao, L. H.; Jin, H. J.; Viswanath, R. N.; Weissmuller, J. Different measures for the capillarity-driven deformation of a nanoporous metal. *EPL* **2010**, *89* (6), 5.

(22) Huber, P.; Busch, M.; Całus, S.; Kityk, A. V. Thermotropic nematic order upon nanocapillary filling. *Phys. Rev. E* **2013**, *87* (4), 042502.
(23) Shkolin, A. V.; Fomkin, A. A.; Sinitsyn, V. A. Adsorption-induced deformation of AUK microporous carbon adsorbent in adsorption of n-pentane. *Prot. Met. Phys. Chem. Surf.* **2012**, *47* (5), 555−561.
(24) Ustinov, E. A.; Do, D. D. Effect of adsorption deformation on thermodynamic characteristics of a fluid in slit pores at sub-critical conditions. *Carbon* **2006**, *44* (13), 2652−2663.
(25) Kowalczyk, P.; Furmaniak, S.; Gauden, P. A.; Terzyk, A. P. Carbon dioxide adsorption-induced deformation of microporous carbons. *J. Phys. Chem. C* **2010**, *114* (11), 5126−5133.
(26) Schoen, M.; Paris, O.; Gunther, G.; Muter, D.; Prass, J.; Fratzl, P. Pore-lattice deformations in ordered mesoporous matrices: experimental studies and theoretical analysis. *Phys. Chem. Chem. Phys.* **2010**, *12* (37), 11267−11279.
(27) Pijaudier-Cabot, G.; Vermorel, R.; Miqueu, C.; Mendiboure, B. Revisiting poromechanics in the context of microporous materials. *C. R. Mec.* **2011**, *339* (12), 770−778.
(28) Nguyen, V. T.; Do, D. D.; Nicholson, D. Solid deformation induced by the adsorption of methane and methanol under sub- and supercritical conditions. *J. Colloid Interface Sci.* **2012**, *388*, 209−218.
(29) Kresge, C. T.; Leonowicz, M. E.; Roth, W. J.; Vartuli, J. C.; Beck, J. S. Ordered mesoporous molecular-sieves synthesized by a liquid-crystal template mechanism. *Nature* **1992**, *359* (6397), 710−712.
(30) Zhao, D. Y.; Feng, J. L.; Huo, Q. S.; Melosh, N.; Fredrickson, G. H.; Chmelka, B. F.; Stucky, G. D. Triblock copolymer syntheses of mesoporous silica with periodic 50 to 300 angstrom pores. *Science* **1998**, *279* (5350), 548−552.
(31) Landers, J.; Gor, G. Y.; Neimark, A. V. Density functional theory methods for characterization of porous materials. *Colloids Surf., A* **2013**, DOI: 10.1016/j.colsurfa.2013.01.007.
(32) Reichenauer, G.; Scherer, G. W. Nitrogen adsorption in compliant materials. *J. Non-Cryst. Solids* **2000**, *277* (2−3), 162−172.
(33) Ravikovitch, P. I.; Neimark, A. V. Density functional theory model of adsorption deformation. *Langmuir* **2006**, *22* (26), 10864−10868.
(34) Kowalczyk, P.; Ciach, A.; Neimark, A. V. Adsorption-induced deformation of microporous carbons: Pore size distribution effect. *Langmuir* **2008**, *24* (13), 6603−6608.
(35) Gor, G. Y.; Neimark, A. V. Adsorption-induced deformation of mesoporous solids: Macroscopic approach and density functional theory. *Langmuir* **2011**, *27* (11), 6926−6931.
(36) Derjaguin, B. V. A theory of capillary condensation in the pores of sorbents and of other capillary phenomena taking into account the disjoining action of polymolecular liquid films. *Acta Physicochim. URSS* **1940**, *12*, 181.
(37) Broekhoff, J. C. P.; de Boer, J. H. Studies on pore systems in catalysts: IX. Calculation of pore distributions from the adsorption branch of nitrogen sorption isotherms in the case of open cylindrical pores A. Fundamental equations. *J. Catal.* **1967**, *9* (1), 8−14.
(38) Broekhoff, J. C. P.; De Boer, J. H. Studies on pore systems in catalysts: X. Calculations of pore distributions from the adsorption branch of nitrogen sorption isotherms in the case of open cylindrical pores B. Applications. *J. Catal.* **1967**, *9* (1), 15−27.
(39) Frenkel, J. I. *Kinetic Theory of Liquids*; Oxford University Press: London, 1946.
(40) Halsey, G. Physical adsorption on non-uniform surfaces. *J. Chem. Phys.* **1948**, *16* (10), 931−937.
(41) Hill, T. L.; Frankenburg, W. G.; Komarewsky, V. I.; Rideal, E. K. *Theory of Physical Adsorption*; Academic Press: New York, 1952; Vol. *4*, pp 211−258.
(42) Pashley, R. M. Hydration forces between mica surfaces in electrolyte solutions. *Adv. Colloid Interface Sci.* **1982**, *16* (1), 57−62.
(43) Russo, P. A.; Ribeiro Carrott, M. M. L.; Carrott, P. J. M. Hydrocarbons adsorption on templated mesoporous materials: effect of the pore size, geometry and surface chemistry. *New J. Chem.* **2011**, *35* (2), 407−416.
(44) Russo, P. A.; Ribeiro Carrott, M. M. L.; Carrott, P. J. M. Trends in the condensation/evaporation and adsorption enthalpies of volatile organic compounds on mesoporous silica materials. *Microporous Mesoporous Mater.* **2012**, *151*, 223−230.
(45) Carrott, P. J. M.; Roberts, R. A.; Sing, K. S. W. Adsorption of neopentane by nonporous carbons and silicas. *Langmuir* **1988**, *4* (3), 740−743.
(46) Gregg, S. J.; Sing, K. S. W. *Adsorption, Surface Area and Porosity*; Academic Press: London, 1982.
(47) Rouquerol, F.; Rouquerol, J.; Sing, K. *Adsorption by Powders and Porous Solids: Principles, Methodology and Applications*; Academic Press: London, 1999.
(48) Jahnert, S.; Chavez, F. V.; Schaumann, G. E.; Schreiber, A.; Schonhoff, M.; Findenegg, G. H. Melting and freezing of water in cylindrical silica nanopores. *Phys. Chem. Chem. Phys.* **2008**, *10* (39), 6039−6051.
(49) Findenegg, G. H.; Jahnert, S.; Muter, D.; Paris, O. Analysis of pore structure and gas adsorption in periodic mesoporous solids by in situ small-angle X-ray scattering. *Colloid Surf., A* **2010**, *357* (1−3), 3−10.
(50) Neimark, A. V.; Ravikovitch, P. I.; Vishnyakov, A. Bridging scales from molecular simulations to classical thermodynamics: density functional theory of capillary condensation in nanopores. *J. Phys.: Condens. Matter* **2003**, *15* (3), 347−365.
(51) Derjaguin, B. V.; Churaev, N. V.; Muller, V. M. *Surface Forces*; Consultants Bureau: New York, 1987.
(52) Churaev, N. V.; Zorin, Z. M. Wetting films. *Adv. Colloid Interface Sci.* **1992**, *40*, 109−146.
(53) Schlangen, L. J. M.; Koopal, L. K.; Stuart, M. A. C.; Lyklema, J.; Robin, M.; Toulhoat, H. Thin hydrocarbon and water films on bare and methylated silica: Vapor adsorption, wettability, adhesion, and surface forces. *Langmuir* **1995**, *11* (5), 1701−1710.
(54) Ravikovitch, P. I.; Vishnyakov, A.; Neimark, A. V.; Ribeiro Carrott, M. M. L.; Russo, P. A.; Carrott, P. J. Characterization of micro-mesoporous materials from nitrogen and toluene adsorption: Experiment and modeling. *Langmuir* **2006**, *22* (2), 513−516.
(55) Kowalczyk, P.; Jaroniec, M.; Terzyk, A. P.; Kaneko, K.; Do, D. D. Improvement of the Derjaguin-Broekhoff-de Boer theory for capillary condensation/evaporation of nitrogen in mesoporous systems and its implications for pore size analysis of MCM-41 silicas and related materials. *Langmuir* **2005**, *21* (5), 1827−1833.
(56) Churaev, N. V.; Derjaguin, B. V. Inclusion of structural forces in the theory of stability of colloids and films. *J. Colloid Interface Sci.* **1985**, *103* (2), 542−553.
(57) Weissmueller, J.; Duan, H. L.; Farkas, D. Deformation of solids with nanoscale pores by the action of capillary forces. *Acta Mater.* **2010**, *58* (1), 1−13.
(58) Whipple, F. J. W. The theory of the hair hygrometer. *Proc. Phys. Soc. London* **1921**, *34* (1), i.
(59) Froba, A. P.; Pellegrino, L. P.; Leipertz, A. Viscosity and surface tension of saturated n-pentane. *Int. J. Thermophys.* **2004**, *25* (5), 1323−1337.
(60) Dendooven, J.; Devloo-Casier, K.; Levrau, E.; Van Hove, R.; Sree, S. P.; Baklanov, M. R.; Martens, J. A.; Detavernier, C. In situ monitoring of atomic layer deposition in nanoporous thin films using ellipsometric porosimetry. *Langmuir* **2012**, *28* (8), 3852−3859.
(61) Horikawa, T.; Do, D. D.; Nicholson, D. Capillary condensation of adsorbates in porous materials. *Adv. Colloid Interface Sci.* **2011**, *169* (1), 40−58.
(62) Coasne, B.; Haines, J.; Levelut, C.; Cambon, O.; Santoro, M.; Gorelli, F.; Garbarino, G. Enhanced mechanical strength of zeolites by adsorption of guest molecules. *Phys. Chem. Chem. Phys.* **2011**, *13* (45), 20096−20099.
(63) Santander, J. E.; Tsapatsis, M.; Auerbach, S. M. Simulating adsorptive expansion of zeolites: Application to biomass-derived solutions in contact with silicalite. *Langmuir* **2013**, *29* (15), 4866−4876.